Accurate Recovery of H I Velocity Dispersion from Radio Interferometers

Ianjamasimanana, R.; de Blok, W. J. G.; Heald, George H.

Published in:
The Astronomical Journal

DOI:
10.3847/1538-3881/aa6717

Publication date:
2017

The Astronomical Journal, 153:213 (13pp), 2017 May https://doi.org/10.3847/1538-3881/aa6717

Accurate Recovery of H I Velocity Dispersion from Radio Interferometers

R. Ianjamasimanana[1], W. J. G. de Blok[2,3,4], and George H. Heald[4,5]
[1] Max-Planck Institut für Astronomie, Königstuhl 17, D-69117, Heidelberg, Germany; roger@mpia.de
[2] Netherlands Institute for Radio Astronomy (ASTRON), Postbus 2, 7990 AA Dwingeloo, The Netherlands
[3] Astrophysics, Cosmology and Gravity Centre, Department of Astronomy, University of Cape Town, Private Bag X3, Rondebosch 7701, South Africa; blok@astron.nl
[4] Kapteyn Astronomical Institute, University of Groningen, P.O. Box 800, 9700 AV, Groningen, The Netherlands; George.Heald@csiro.au
[5] CSIRO Astronomy and Space Science, 26 Dick Perry Avenue, Kensington WA 6151, Australia
Received 2016 August 24; revised 2017 March 11; accepted 2017 March 13; published 2017 April 14

Abstract

Gas velocity dispersion measures the amount of disordered motion of a rotating disk. Accurate estimates of this parameter are of the utmost importance because the parameter is directly linked to disk stability and star formation. A global measure of the gas velocity dispersion can be inferred from the width of the atomic hydrogen (H I) 21 cm line. We explore how several systematic effects involved in the production of H I cubes affect the estimate of H I velocity dispersion. We do so by comparing the H I velocity dispersion derived from different types of data cubes provided by The H I Nearby Galaxy Survey. We find that residual-scaled cubes best recover the H I velocity dispersion, independent of the weighting scheme used and for a large range of signal-to-noise ratio. For H I observations, where the dirty beam is substantially different from a Gaussian, the velocity dispersion values are overestimated unless the cubes are cleaned close to (e.g., ∼1.5 times) the noise level.

Key words: galaxies: fundamental parameters – galaxies: ISM – ISM: kinematics and dynamics – line: profiles – methods: data analysis

1. Introduction

The random motion of gas in galaxies can be traced from the width of the ubiquitous 21 cm line of atomic hydrogen (H I). The amount of the disordered motion, the gas velocity dispersion, provides valuable information on the physical properties of the gas such as its ability to collapse and form stars, the energy balance, and the phase structure of the gas (Schaye 2004; Tamburro et al. 2009; O'Brien et al. 2010; Ianjamasimanana et al. 2012; Stilp et al. 2013). This parameter is usually determined by fitting H I profiles with an assumed model, e.g., a single or a double Gaussian function, a Gauss–Hermite polynomial, or a Lorentzian (Braun 1997; Young et al. 2003; Ianjamasimanana et al. 2012). Instead of assuming a model, the intensity-weighted standard deviation of the line-of-sight velocities has also been used as a measure of H I velocity dispersion (e.g., Tamburro et al. 2009).

An accurate determination of the H I velocity dispersion is limited by the ability of the imaging process to recover the intrinsic shapes of the H I line profiles. In radio interferometry, the source intensity distribution is not completely sampled by the telescope array. Therefore, to recover the missing values in the (u, v) data and reconstruct the true image of the source, the telescope point spread function (PSF or dirty beam) needs to be deconvolved from the observed (dirty) image. As will be explained in detail later, the recovered image from a deconvolution algorithm is obtained by adding a deconvolved map of the model of the source brightness distribution (derived down to a certain flux) to a map containing the remaining emission, usually assumed to be noise (the residual map).

The width of the H I velocity profiles means that typically they will be spread over several velocity channels. The faint outer wings of these profiles can thus appear in adjacent channels but with intensities below the threshold for cleaning. The residual image will then still contain faint residual emission corresponding to these wings. In this paper, we investigate what the effect of this uncleaned, residual emission is on measurements of the velocity dispersion and find that it leads to an overestimate of this parameter. Here we focus on data obtained as part of The H I Nearby Galaxy Survey (THINGS; Walter et al. 2008), but our conclusions will apply to all H I observations where the dirty beam is substantially different from a Gaussian, such as is the case with multi-configuration Very Large Array (VLA) observations. This includes recent surveys, such as Local Irregulars That Trace Luminosity Extremes: The H I Nearby Galaxy Survey (Little THINGS; Hunter et al. 2012), VLA survey of Advanced Camera for Surveys Nearby Galaxy Survey Treasury galaxies (VLA-ANGST; Ott et al. 2012), and Survey of H I in Extremely Low-mass Dwarfs (SHIELD; Cannon et al. 2011). This study is also relevant for other arrays that produce a non-Gaussian dirty beam, e.g., the Atacama Large Millimeter/submillimeter Array, meaning the results could also be relevant for molecular line velocity dispersions.

In Section 2, we give background on the weighting of visibilities and cleaning processes. In Section 3, we describe the analysis goal and method. In Section 4, we compare H I velocity dispersion from different types of data cubes. In Section 5, we investigate the type of data cubes that should be used in H I velocity dispersion analysis. In Section 6, we discuss our results and conclusions.

2. Background

Interferometric observations of radio astronomical sources provide noisy samples of the complex visibility function of the sources at discrete locations in the (u, v) plane (Cornwell 2008), where u and v are the baseline vectors projected onto a plane perpendicular to the source direction. Deconvolution algorithms attempt to recover the image information (missing values) in the un-sampled (u, v) plane. The inverse Fourier transform (FT) of the sampled visibility function,

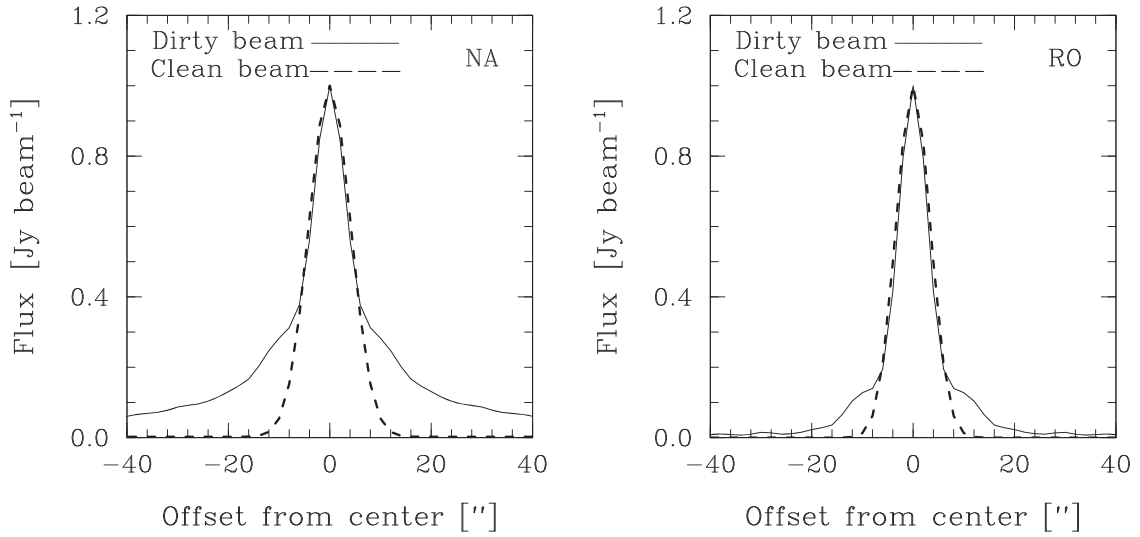

Figure 1. Dirty and clean beams of the THINGS natural (left panel) and the robust (right panel) weighted data cubes of NGC 3184.

$S(u, v)\ V(u, v)$, is called *the dirty image*, I_D:

$$I_D = \mathcal{F}^{-1}(S(u, v)\, V(u, v)), \quad (1)$$

where $S(u, v)$ is a sampling function and $V(u, v)$ is the visibility function. Using the Fourier convolution theorem, which states that the FT of the product of two functions is the convolution of the FT of the two functions, Equation (1) becomes:

$$I_D = \mathcal{F}^{-1}(S(u, v)) \otimes \mathcal{F}^{-1}(V(u, v)). \quad (2)$$

In radio astronomy jargon, $\mathcal{F}^{-1}(S(u, v))$ is called *the dirty beam*. The true image is the inverse FT of the visibility function, $\mathcal{F}^{-1}(V(u, v))$. A deconvolution algorithm involves solving for the true image given the dirty beam and the dirty image. To get the dirty image from the sampled visibility functions, a fast Fourier transform (FFT) is usually preferable over the *simple* FT due to its computational speed. However, FFT requires that the sample visibilities are on a regularly spaced grid (cell) (e.g., Yatawatta 2014). In the image reconstruction and gridding process, a weighting function is usually applied to the sampled visibility function to, e.g., maximize point source sensitivity or to minimize sidelobe levels. If $W(u, v)$ is a weighting function, then Equation (1) becomes:

$$I_D = \mathcal{F}^{-1}(W(u, v)\, S(u, v)\, V(u, v)). \quad (3)$$

Many forms of weighting functions have been developed for different science goals. This paper discusses the effects of using different weighting schemes in the derivation of H I velocity dispersion. Natural, uniform and robust (or Briggs) weightings are widely known weighting schemes in radio interferometry. The natural weighting gives a weight of $1/\sigma_i^2$ on visibility i, where σ_i^2 is the noise variance of that visibility. In most cases, the noise is roughly similar for all visibilities and thus each (u, v) point gets approximately the same weight. Due to the gridding, (u, v) cells at shorter baselines get more weight as the inner parts of the (u, v) plane have a higher density of (u, v) points (i.e., measured visibilities). Thus, natural weighting offers the best surface brightness sensitivity and minimum noise, but at the cost of a larger beam size. For uniform weighting, a given cell in the (u, v) plane gets a weight of $1/\rho_{(u,v)}$, where $\rho_{(u,v)}$ is the density of the (u, v) points in the cell. Given that the density of the (u, v) points is usually lower at larger baselines, the latter are weighted more, resulting in better resolution but lower sensitivity (short baselines are de-emphasized), and therefore an increased rms noise. The uniform weighting gives better (i.e., lower) side lobes than the natural weighting. Robust weighting combines the advantage offered by the natural weighting and the uniform weighting. It gives a resolution approaching that of a uniform weighting, with only a modest cost in sensitivity (Briggs 1995). After gridding the sample visibilities and performing an FFT on Equation (3), the obtained dirty image needs to be deconvolved to get an estimate of the true image. CLEAN, first described by Högbom (1974), is among the widely used algorithms for this purpose. There have been many variants of CLEAN since its inception, most of them aiming to improve computational efficiency and performance with respect to extended structure. The original CLEAN algorithm, also called classical CLEAN or delta function CLEAN, assumes that the true image brightness distribution can be well represented by a collection of point sources. The algorithm iteratively searches for the locations and strengths of the point sources and iteratively subtracts them using the shape of the dirty beam to generate a *residual map* and a *clean component list*. It is common practice to convolve the clean component list with an idealized "CLEAN beam" (e.g., usually a Gaussian with a FWHM matching that of the central component of the dirty beam Rich et al. 2008). The convolved clean component list is then added to the residual map to obtain the final restored image, which is a plausible representation of the true image. Thus, the CLEANed map is a combination of two maps, imaged with two different beams. This paper explores the effects of this on measurements of the H I velocity dispersion.

Table 1
The Sample Galaxies

Galaxy	Weighting	B_{maj} ($''$)	B_{min} ($''$)	Ch. Width (km s^{-1})
1	2	3	4	5
NGC 628	NA	11.88	9.30	2.6
	RO	6.8	5.57	⋯
NGC 925	NA	5.94	5.71	2.6
	RO	4.85	4.65	⋯
NGC 2366	NA	13.10	11.85	2.6
	RO	6.96	5.94	⋯
NGC 2403	NA	8.75	7.65	5.2
	RO	6.01	5.17	⋯
Ho II	NA	13.74	12.57	2.6
	RO	6.95	6.05	⋯
M81 dwA	NA	15.87	14.23	1.3
	RO	7.79	6.27	⋯
DDO 53	NA	11.75	9.53	2.6
	RO	6.34	5.67	⋯
NGC 2903	NA	15.27	13.32	5.2
	RO	8.66	6.43	⋯
Ho I	NA	14.66	12.73	2.6
	RO	7.78	6.03	⋯
NGC 2976	NA	7.41	6.42	5.2
	RO	5.25	4.88	⋯
NGC 3184	NA	7.51	6.93	2.6
	RO	5.33	5.11	⋯
NGC 3198	NA	13.01	11.56	5.2
	RO	7.64	5.62	⋯
IC 2574	NA	12.81	11.90	2.6
	RO	5.93	5.48	⋯
NGC 3351	NA	9.94	7.15	5.2
	RO	6.26	5.20	⋯
NGC 3621	NA	15.95	10.24	5.2
	RO	10.50	5.68	⋯
NGC 4214	NA	14.69	13.87	1.3
	RO	7.41	6.35	⋯
NGC 4736	NA	10.22	9.07	5.2
	RO	5.96	5.55	⋯
DDO 154	NA	14.09	12.62	2.6
	RO	7.94	6.27	⋯
NGC 5055	NA	10.06	8.66	5.2
	RO	5.78	5.26	⋯
NGC 5236	NA	15.16	11.44	2.6
	RO	10.40	5.60	⋯
NGC 6946	NA	6.04	5.61	2.6
	RO	4.93	4.51	⋯
NGC 7793	NA	15.60	10.85	2.6
	RO	10.37	5.39	⋯

Note. Column 1: Name of galaxy; Column 2: NA: Natural weighting; RO: Robust weighting; Column 3/4: major and minor axis of synthesized beam in arcsec; Column 5: Channel width.

3. Goal and Method

3.1. Residual Scaling

Naively, one would expect that the flux of a channel map is obtained by simply adding the flux of the cleaned map to that of the residual map:

$$F = C + R, \tag{4}$$

where C is the cleaned flux and R is the residual flux. However, C and R have different units (C is in Jy/clean beam and R in Jy/dirty beam) and depending on the configuration of the array, the shape of the dirty beam can be strongly non-Gaussian and more extended than the clean beam. This mismatch in shape between the dirty beam and the clean beam leads to an overestimate of the flux density if the clean beam parameters are used to determine the flux of sources containing both cleaned and residual emission. We illustrate in Figure 1 how the dirty beam and the clean beam differ from each other in typical multi-configuration observations with the VLA. To account for the difference in area between the clean beam and the dirty beam, the flux of the residual must be scaled by a scaling factor ϵ:

$$F\,(\text{true}) = C + \epsilon\ R, \tag{5}$$

where F(true) is the corrected flux and ϵ is a correction factor that accounts for the ratio between the clean beam area and the dirty beam area (Jorsater & van Moorsel 1995). Theoretically, due to the absence of zero spacing in interferometric data, the dirty beam integral and the total flux density of the dirty image are zero as there are equal amounts of positive and negative flux in the dirty image. In practice, the positive flux is mostly concentrated in the main lobe of the dirty beam and, for the purposes of residual scaling, one has to choose a region (box) centered on the main lobe over which to integrate the dirty beam and ensure most of the flux in the main lobe is captured. The residual scaling method is included in the AIPS[6] task IMAGR and more technical aspects are presented there. As described in Walter et al. (2008), the calculation of the flux in the main lobe of the THINGS dirty beam was done inside a box with a half-width of 50 pixels (75″) in R.A. and in decl. This box was chosen as it encompasses the larger part of the main lobe of the THINGS dirty beam while still well within its first negative sidelobe. This choice is appropriate for all of the THINGS galaxies as they have all been observed in the same manner and with the same set-up, meaning their dirty beams are all very similar. A quantitative analysis of the uncertainties associated with this choice of box size and with the use of a different dirty beam area has not been performed, and is beyond the scope of this paper. However, initial testing prior to the reduction of the THINGS data as presented in Walter et al. (2008) indicates that residual-scaling results do not critically depend on the box size (F. Walter 2017, private communication). Note that the residual scaling affects the noise and thus it should only be used for flux measurements in areas with genuine emission (Rich et al. 2008; Walter et al. 2008; Ott et al. 2012). For this reason, the THINGS residual-scaled cubes are blanked in areas judged to be devoid of emission. The criterion used by THINGS is that genuine emission must be present in at least three consecutive channels at or above a level of 2σ in standard cubes convolved to 30″ resolution. These cubes are then used as masks to blank areas containing only noise. While residual scaling has been widely used to get more accurate flux values (e.g., Walter et al. 2008), the effects its presence or absence has on H I velocity dispersion have not yet been well explored. Stilp et al. (2013) first noticed the difference between H I velocity dispersion derived from flux-

[6] The Astronomical Image Processing System (AIPS) has been developed by the National Radio Astronomy Observatory (NRAO).

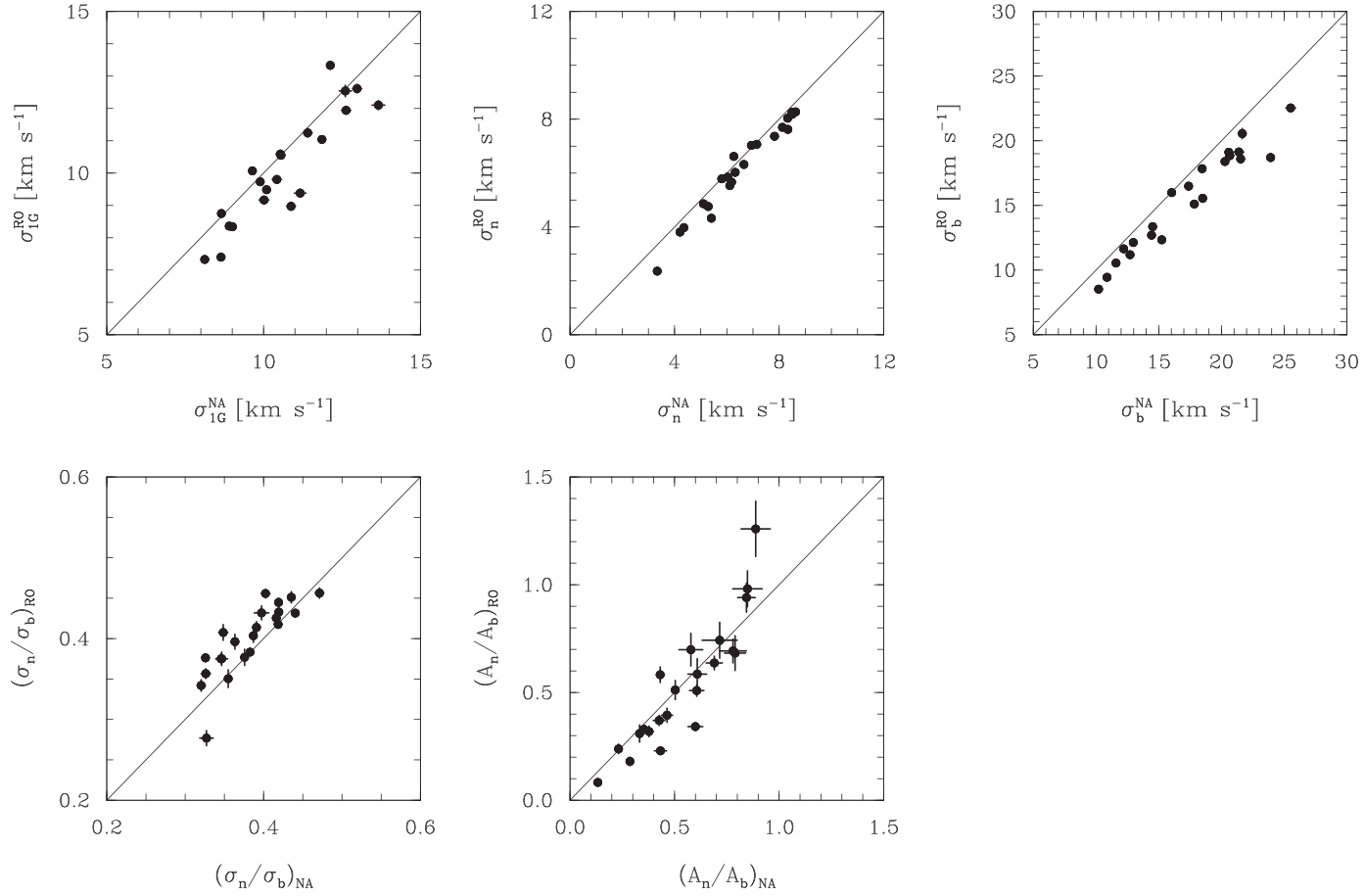

Figure 2. Comparison of super profile parameters from natural non-residual-scaled (NA) and robust non-residual-scaled (RO) data cubes; σ_{1G}: velocity dispersion from a single Gaussian fit; σ_n: narrow component velocity dispersion; σ_b: broad component velocity dispersion; A_n/A_b: ratio of linestrength (or flux ratio) between the narrow and broad components.

rescaled cubes and standard cubes obtained using multi-configuration VLA observations. This paper makes a thorough comparison of H I velocity dispersions derived from residual-scaled cubes and non-residual-scaled cubes from THINGS.

3.2. Cleaning Depth

The widely used classical CLEAN algorithm iteratively deconvolves images until the peak residual flux reaches an adopted threshold value. Most major H I surveys of nearby galaxies (e.g., THINGS, Little THINGS, VLA-ANGST) have adopted a cleaning level of 2.5 times the rms noise to prevent noise spikes from being cleaned and to avoid divergence of the CLEAN process. The effects of residual emissions due to the extended wings of the dirty beam can be minimized by deeply cleaning the data, but this can be computationally expensive and could introduce additional artefacts. Again, the choice of the cleaning depth is driven by obtaining a reasonable flux estimate but its effects on the measurement of H I velocity dispersion have not been quantified previously. This analysis explores how cleaning depth affects H I velocity dispersion and investigates a number of methods that can lead to a more accurate determination of the velocity dispersion.

3.3. Weighting of Visibilities

The choice of weighting scheme in deconvolution algorithms can also affect the measurement of H I velocity dispersion. This is because the dirty beam, which depends on the configuration of the array and the weighting function used, influences the shape of the clean restoring beam and consequently that of the individual velocity profiles in the final restored image. We analyze the effects of weighting of uv-data during image construction on H I velocity dispersion by comparing velocity dispersion from natural and robust weighted data cubes. Finally, using model data cubes, we investigate which type of data cubes should ideally be used for velocity dispersion analysis, or more broadly, analysis of profile widths and shapes. In this paper we focus on using the THINGS data, but note that the conclusions are generally applicable to any observation where the dirty beam differs substantially from a Gaussian. This also implies that for arrays where the dirty beam is close to Gaussian (e.g., the Westerbork Synthesis Radio Telescope, WSRT), the need for residual scaling will be much reduced or absent.

3.4. Sample and Method

This analysis uses 22 galaxies from THINGS. These were selected to be minimally affected by interactions, projection effects or major bulk motions. For further discussion, we refer the reader to Ianjamasimanana et al. (2012). Their names and observational properties are shown in Table 1 (as also given in Walter et al. 2008). The data provided by THINGS include both natural and robust weighted data cubes (with a robust parameter value of 0.5). For each weighting, the

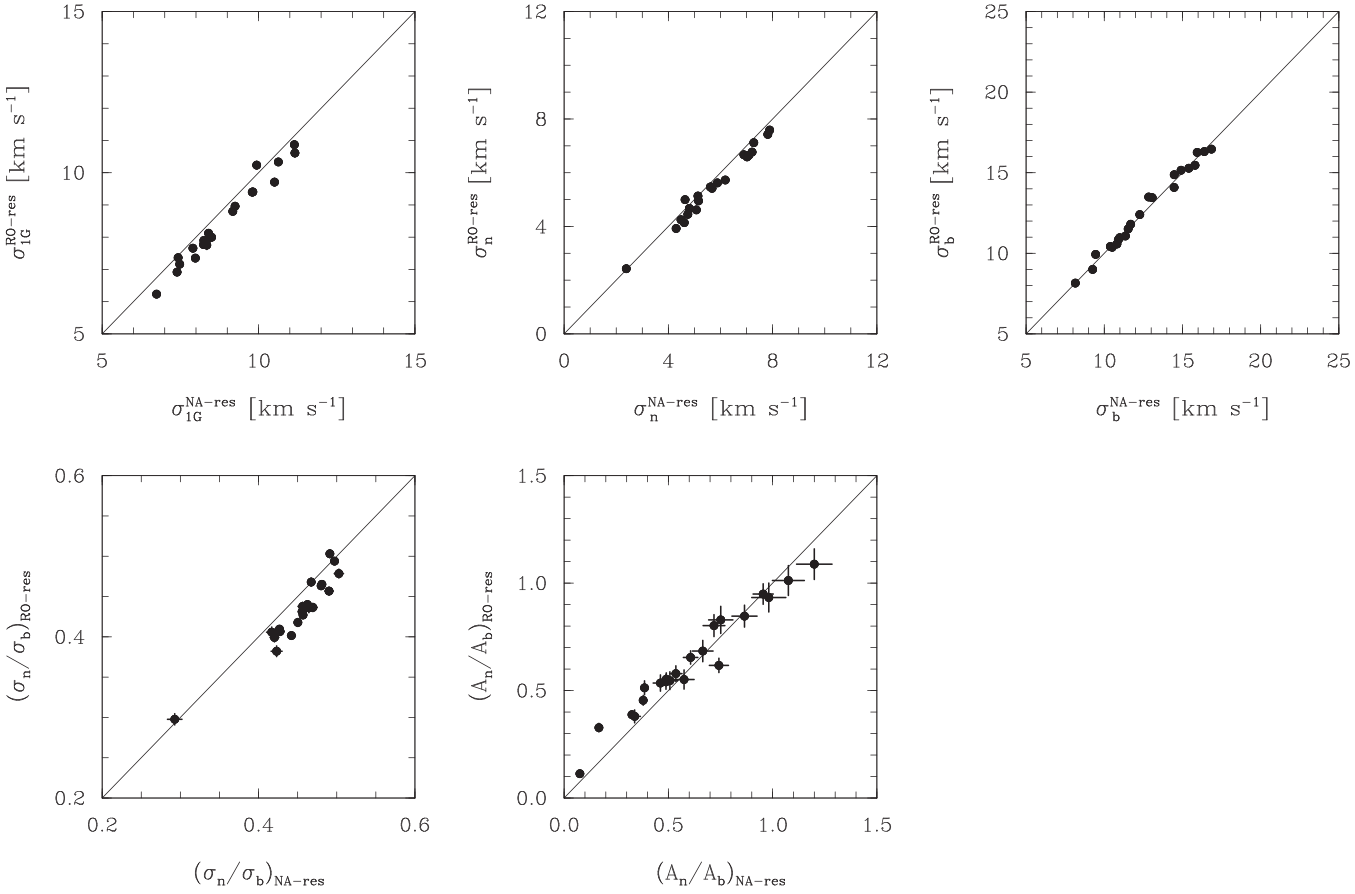

Figure 3. Comparison of super profile parameters from natural residual-scaled (NA-res) and robust residual-scaled (RO-res) data cubes.

non-residual scaled versions are publicly available on the THINGS website (http://www.mpia.de/THINGS/Data.html). The residual-scaled ones are available upon request. Our aim is to characterize the values of the velocity dispersions with high precision. So, as in Ianjamasimanana et al. (2012), individual line profiles with peak amplitude higher than 4 times the rms noise level are aligned to the same reference velocity and summed to derive what we call *super profiles*. We use a velocity field to define the amount of shift per pixel to end up at the same reference velocity. We decompose the high signal-to-noise ratio (S/N) super profiles into narrow and broad Gaussian components and compare the fitted parameters (velocity dispersion, ratio of linestrength or flux ratio between the narrow and broad components) from the different THINGS cubes to assess the effects of deconvolution and residual scaling on H I profile shapes. The narrow component represents high-brightness regions, whereas the broad component contains faint low-level emission where the residual emission contributions can become important. We also describe the results obtained from single Gaussian fits, as generally used in the literature to obtain a more global measure of the dispersion. We remove the effect of missing short spacings, which is inherent to interferometric data and manifests as negative wings in the super profiles, by (simultaneously) including a polynomial background or baseline in the super profile fits. Most of our sample galaxies require a zero or constant background, whereas in a few cases higher-order polynomial fits are needed.

4. Comparing H I Velocity Dispersion from Different Types of Data Cubes

4.1. Natural versus Robust Cubes

Here we compare the super profile parameters of the natural and the robust THINGS data cubes. Figure 2 compares the parameters from the non-residual-scaled version of the cubes. In this case, the natural cubes tend to give higher velocity dispersion values than the robust cubes (∼7% higher for the single Gaussian component, σ_{1G}, and for the narrow component, σ_n, and ∼13% higher for the broad component, σ_b). The ratio of linestrength, or ratio between the narrow and broad component fluxes, A_n/A_b, however, only scatters around the line of equality. Figure 3 presents a comparison of the super profile parameters for the residual-scaled version of the cubes. In this case, the parameters from the natural and the robust cubes are very similar. We conclude that the robust and the natural weighting schemes give similar super profile parameter values in the residual-scaled case, but values differ slightly for the non-residual-scaled cubes.

4.2. Non-residual versus Residual-scaled Cubes

In this section, we compare super profile parameters derived from non-residual-scaled cubes with those from residual-scaled cubes. In Figure 4, we compare super profile parameters of the natural non-residual-scaled cubes (NA) with those of the natural residual-scaled cubes (NA-res). The NA cubes give mean single Gaussian and narrow component velocity

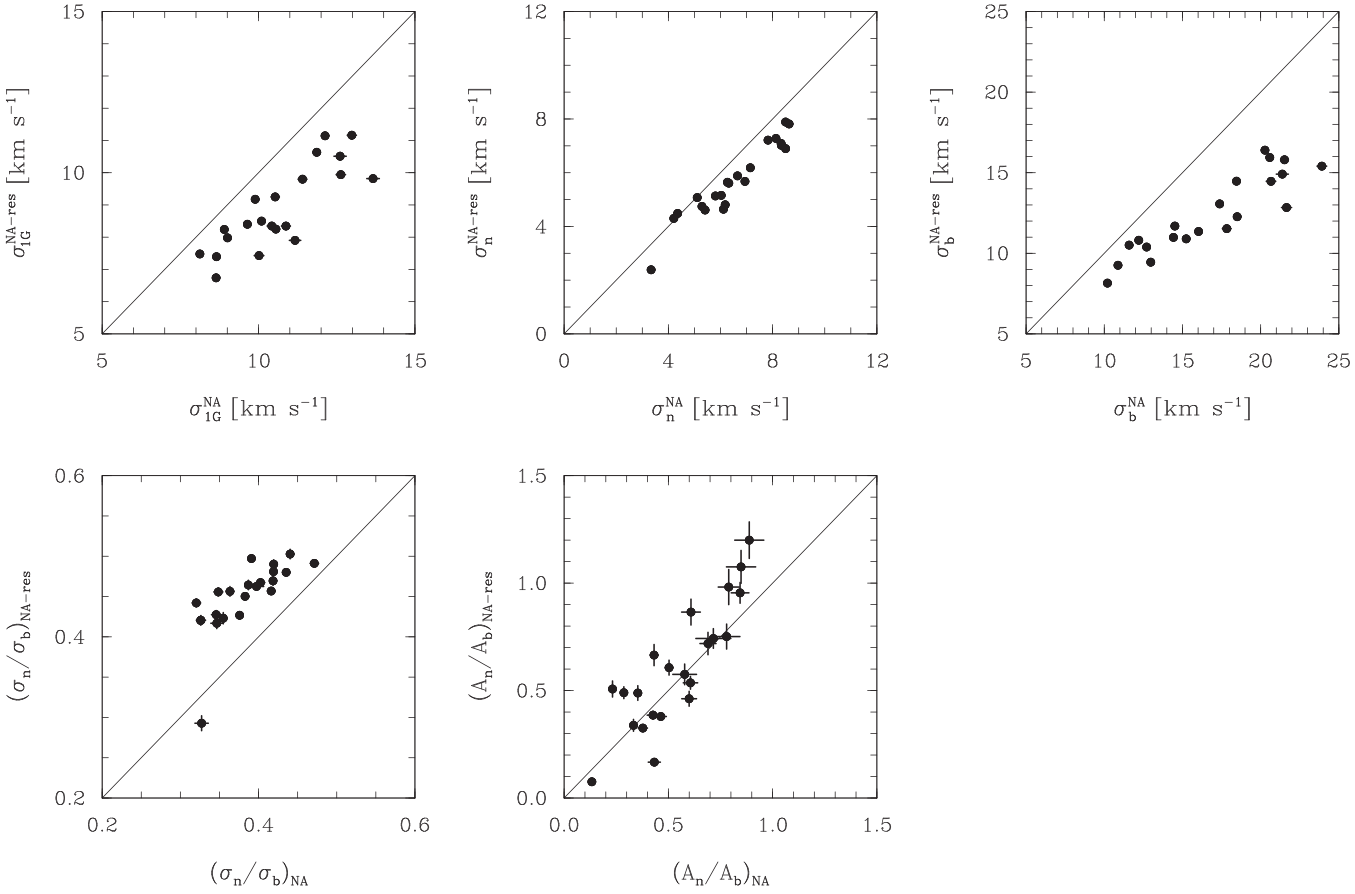

Figure 4. Super profile parameters from natural residual-scaled (NA-res) and natural non-residual-scaled (NA) data cubes.

dispersions that are respectively higher by ∼18% and ∼12% than the NA-res cubes. For the broad component dispersions, the NA cubes give a mean value that is ∼27% higher than that of the NA-res cubes. As a result, the NA cubes give smaller σ_n/σ_b values than the NA-res ones. The A_n/A_b values from the NA and NA-res cubes are similar.

In Figure 5, we compare parameters from robust non-residual-scaled cubes (RO) and robust residual-scaled cubes (RO-res). Here the σ_n from the RO and the RO-res cubes are similar. The mean σ_{1G} and σ_b values from the RO are, on average, ∼16% higher than those of the RO-res, which are much lower than the difference found for the natural-weighted cubes.

In conclusion, the broad component is more sensitive to residual-scaling effects than the narrow and the single Gaussian components. Similarly, the effects of residual scaling are more pronounced for the natural-weighted than for the robust-weighted cubes. Natural non-residual-scaled cubes give broad component dispersion values that are, on average, 10% higher than those of robust non-residual-scaled cubes. Super profile parameters from residual-scaled cubes are similar despite the weighting scheme adopted. In general, the broad component dispersion values from non-residual-scaled cubes are higher than those from residual-scaled cubes.

4.3. Blanked versus Non-blanked Cubes

In the previous section, we have shown that residual-scaled cubes tend to give lower velocity dispersion values than non-oresidual-scaled cubes. Note, however, that as already mentioned in Section 3.1, residual-scaled cubes are also blanked (Walter et al. 2008). So how much of the difference is caused by blanking and how much is due to the residual scaling? To investigate this, we blank the non-residual-scaled cubes using the same blanking mask as the residual-scaled cubes. We do this for both the robust and the natural-weighted data cubes, then derive and fit super profiles from these blanked non-residual-scaled cubes. In Figure 6, we compare the velocity dispersions from the blanked non-residual-scaled cubes with those from the non-blanked non-residual-scaled cubes. In Figure 7, we compare the velocity dispersions from the blanked non-residual-scaled cubes with those from the (already blanked) residual-scaled cubes. We conclude from these two figures that blanking tends to affect only the broad component. This can be understood by the fact that the broad component mostly represents faint emission, which manifests as wings in the super profiles. This low-level emission consists mostly of uncleaned residual emission, which leads to an overestimate of the broad component velocity dispersion when not blanked or residual-scaled. Thus, the difference in broad component velocity dispersion between the residual-scaled cubes and the non-residual-scaled cubes presented in the previous section is partly due to the effects of blanking. For the single Gaussian velocity dispersion, which is most commonly used in the literature, blanking the data cubes does not affect the velocity dispersion, whereas residual scaling the cubes does.

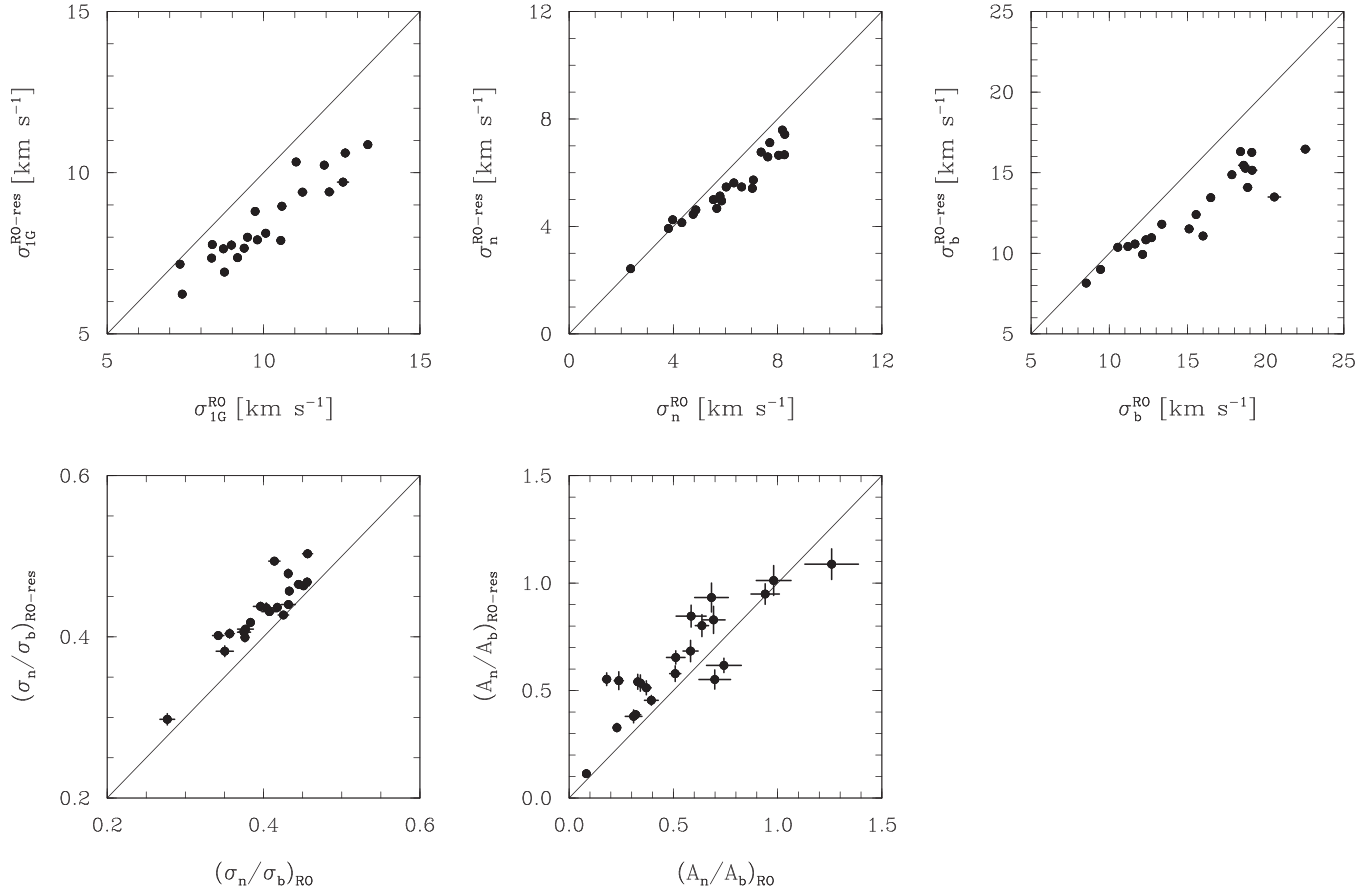

Figure 5. Comparison of the super profile parameters from robust non-residual-scaled (RO) and robust residual-scaled (RO-res) cubes.

4.4. Effects of CLEANing Level on H I Velocity Dispersions for Residual-scaled and Non-residual-scaled Cubes

In the previous sections, we analyzed the effects of weighting and residual scaling on the global measurement of the H I velocity dispersion (i.e., from the entire disk of the galaxies) from data cubes cleaned to 2.5 times the rms noise. However, accurate measurement of the H I velocity dispersion as a function of radius is also important (e.g., for the analysis of disk (in)stability and/or the studies of the shape of the dark matter halo, Petric & Rupen 2007). Here we explore the effects of the choice of CLEAN depth on the measurement of H I velocity dispersion as a function of radius.

We use the dirty image of NGC 3184, a face-on spiral galaxy, and clean it down to 3.5, 2.5, and 1.5 times the rms noise using natural and robust weightings. The 2.5 times rms cube is identical to the standard THINGS cube. We also create blanked non-residual-scaled and (blanked) residual-scaled versions of these cubes. We divide the image of NGC 3184 into series of elliptical annuli with 0.1 r_{25} width (we adopt $r_{25} = 222''$, Walter et al. 2008), with identical orientation parameters (inclination, position angle, and center position) as taken from Walter et al. (2008). We stack individual profiles within each of these annuli and fit the resulting super profiles of the (3.5, 2.5, 1.5) times rms cubes with a single Gaussian function to derive the radial velocity dispersion profiles shown in Figure 8. We show the shapes of the super profiles at a radius of 0.5 r_{25} in Figure 9. We choose NGC 3184 because of its face-on orientation, so projection and beam smearing effects are minimal. For the natural non-residual-scaled cubes, there is a noticeable difference between the velocity dispersion derived from the (3.5, 2.5, 1.5) times rms cubes. This difference is smaller for the robust non-residual-scaled cubes. For residual-scaled data cubes, cleaning level has little to no effect on the derived velocity dispersion. When cleaned down to 1.5 times rms, non-residual-scaled cubes give identical velocity dispersion values to residual-scaled cubes. Blanking seems to affect only the velocity dispersion of the natural non-residual-scaled cubes cleaned to 3.5 times rms. The effects of cleaning level, residual-scaling and blanking on the shapes of the super profiles can be seen in Figure 9.

5. Which Type of Data Cube Should Be Used for Velocity Dispersion Analysis?

In the following, we test which cubes (residual versus non-residual-scaled) best recover an input H I velocity dispersion using simulated data cubes. Using the AIPS task UVMOD, we insert a model in the (u, v) data of NGC 3184. This model consists of a disk with a uniform, constant column density, a diameter of 150″ and a Gaussian velocity distribution. All profiles in the disk have the same mean velocity and velocity width. The model was inserted in an otherwise empty (i.e., containing no line-signal) part of the NGC 3184 (u, v) data set. This data set was then Fourier transformed and CLEANed following the THINGS data reduction procedure. As the model is embedded in the actual, observed (u, v) data, the noise level in the resulting cube is identical to that in the original THINGS cube. For the NGC 3184 data used here the value is 0.36 mJy beam^{-1}. We stop at the cleaning level adopted by THINGS

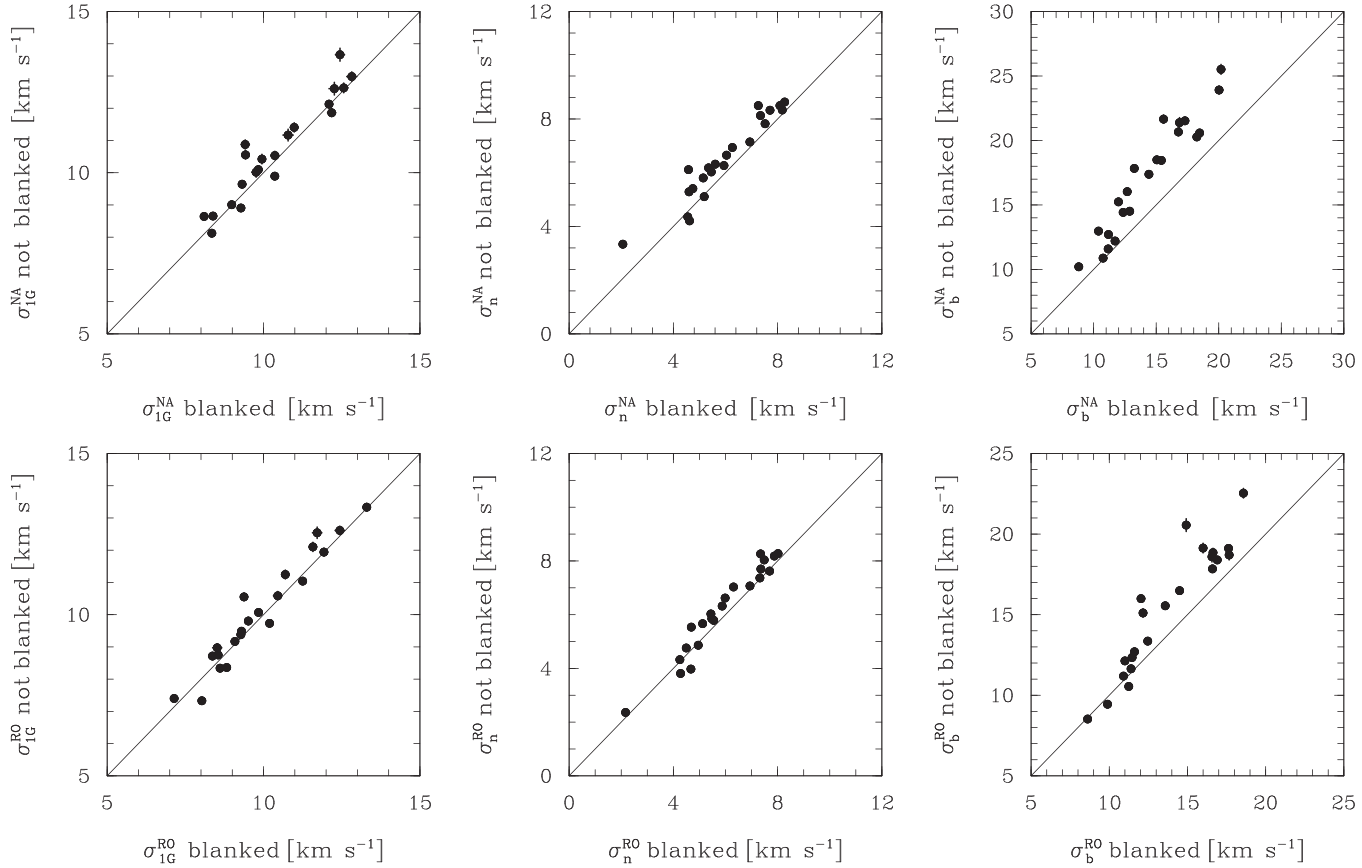

Figure 6. Blanked non-residual-scaled cubes vs. non-blanked non-residual-scaled cubes.

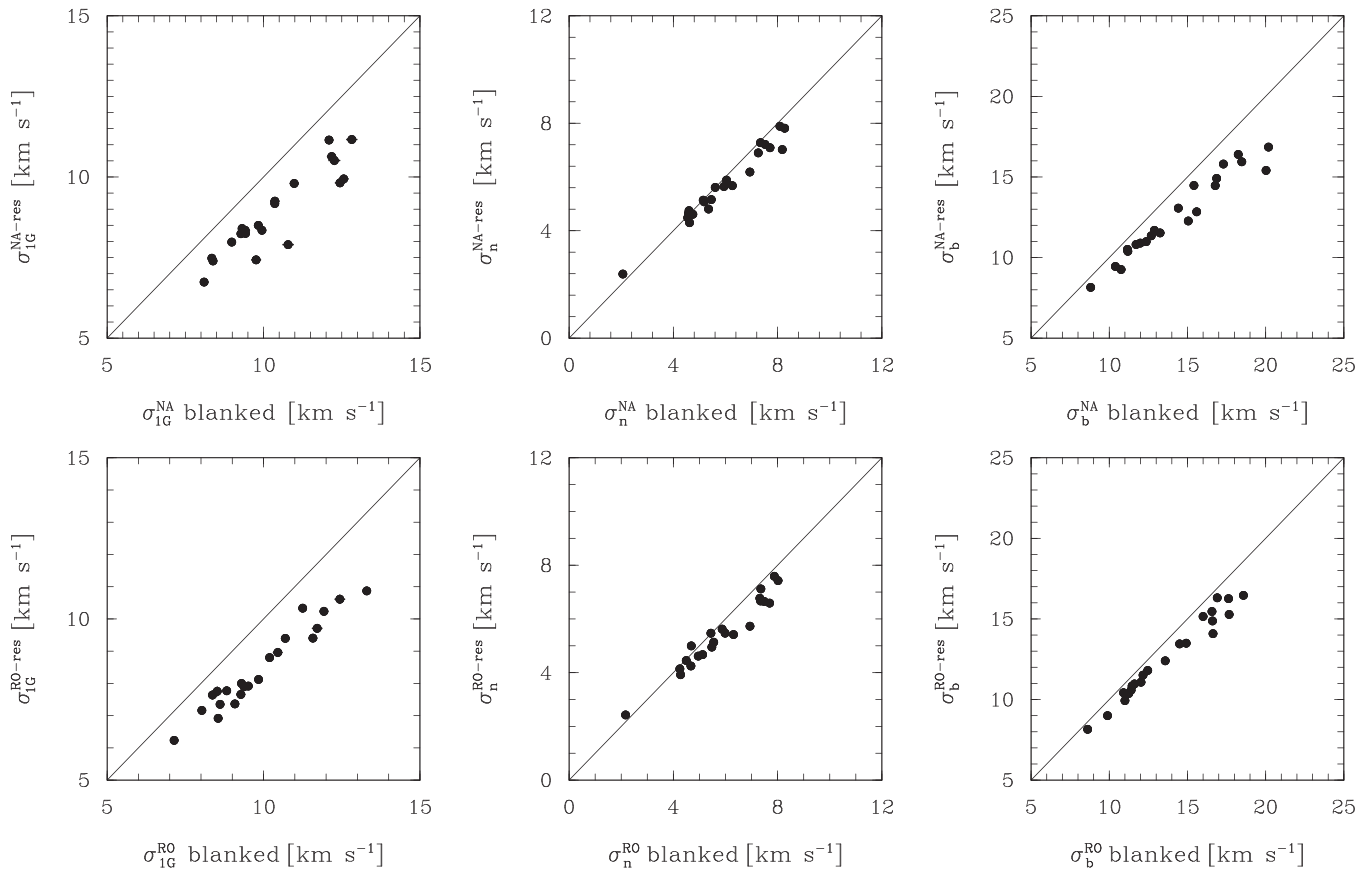

Figure 7. Blanked non-residual-scaled cubes vs. blanked residual-scaled cubes.

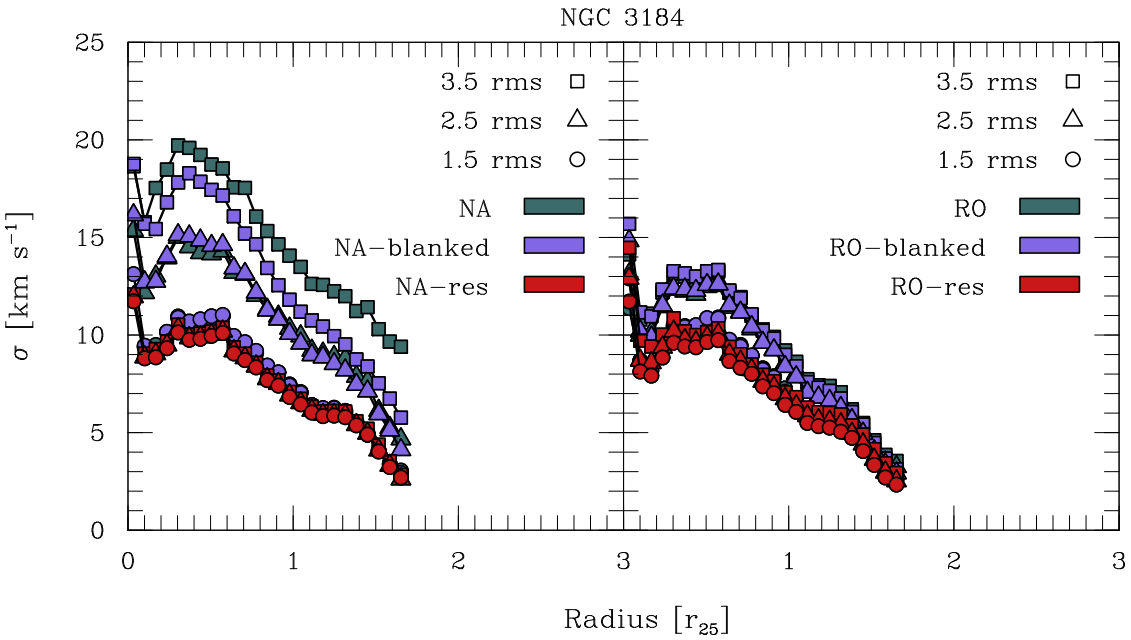

Figure 8. Single Gaussian radial velocity dispersion profiles of NGC 3184 using different weighting schemes and cleaning depths. Different symbols represent different cleaning levels. Squares: 3.5 times rms; triangles: 2.5 times rms; circles: 1.5 times rms. Green: non-residual-scaled cubes (no blanking applied); purple: non-residual-scaled and blanked cubes; red: residual-scaled cubes. Left panel: natural-weighted data cubes; right panel: robust-weighted data cubes.

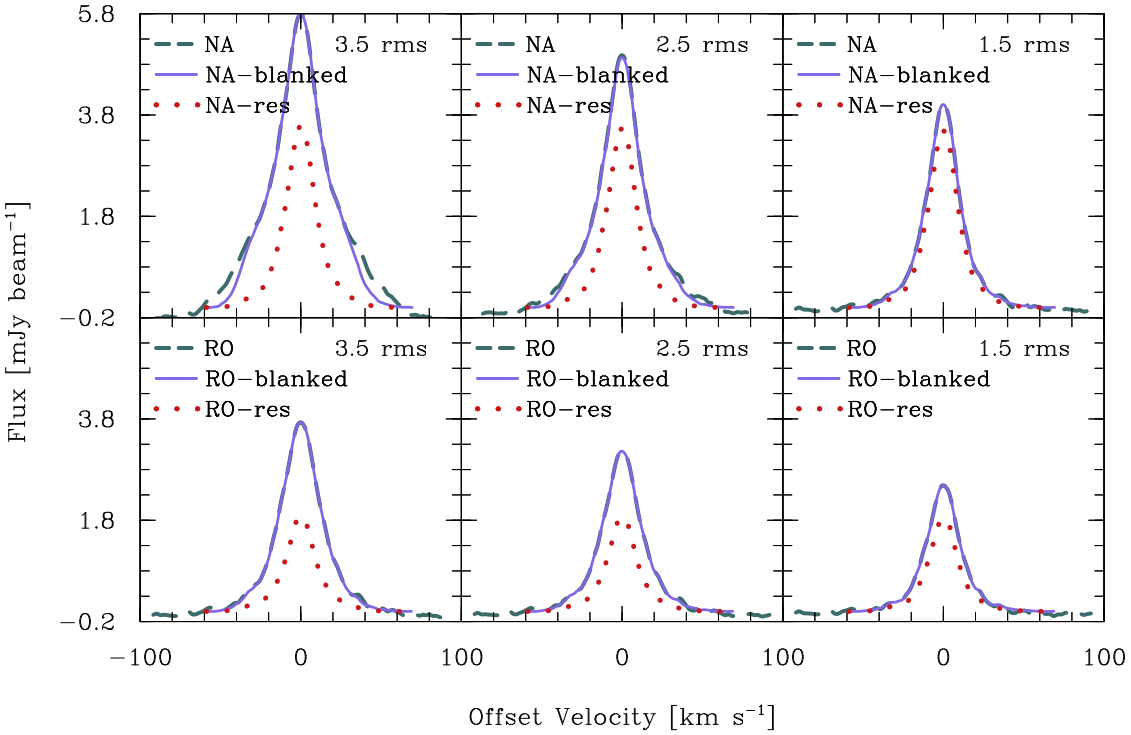

Figure 9. Super profile shapes from non-residual-scaled (green dashed lines: not blanked; purple solid lines: blanked) and residual-scaled (red dotted lines) data cubes of NGC 3184 in annulus of $R \sim 0.5\ r_{25}$ and $W \sim 0.1\ r_{25}$. The top panels are profiles from natural-weighted data cubes and the bottom panels are profiles from robust-weighted data cubes. From left to right, the data cubes are cleaned down to a level of (3.5, 2.5, 1.5) times rms.

(2.5 times rms; Walter et al. 2008) and we use the natural weighting scheme. We create residual and non-residual-scaled version of the simulated cubes. Note that the model spectra are already lined up in velocity; therefore, in constructing the super profiles, no shifting of individual profiles was needed. We simply extracted the profiles at the location of the model disk and summed them. For the model residual-scaled cubes, no additional manual blanking of channel maps was needed. As the profiles are already lined up at known velocities, we simply only consider the velocity range where the profiles are visible.

5.1. Effects of Residual Scaling on Second Moment Values and Single Gaussian Dispersion

In this section, we quantify the effects of low-level uncleaned emission on the derivation of H I velocity dispersion

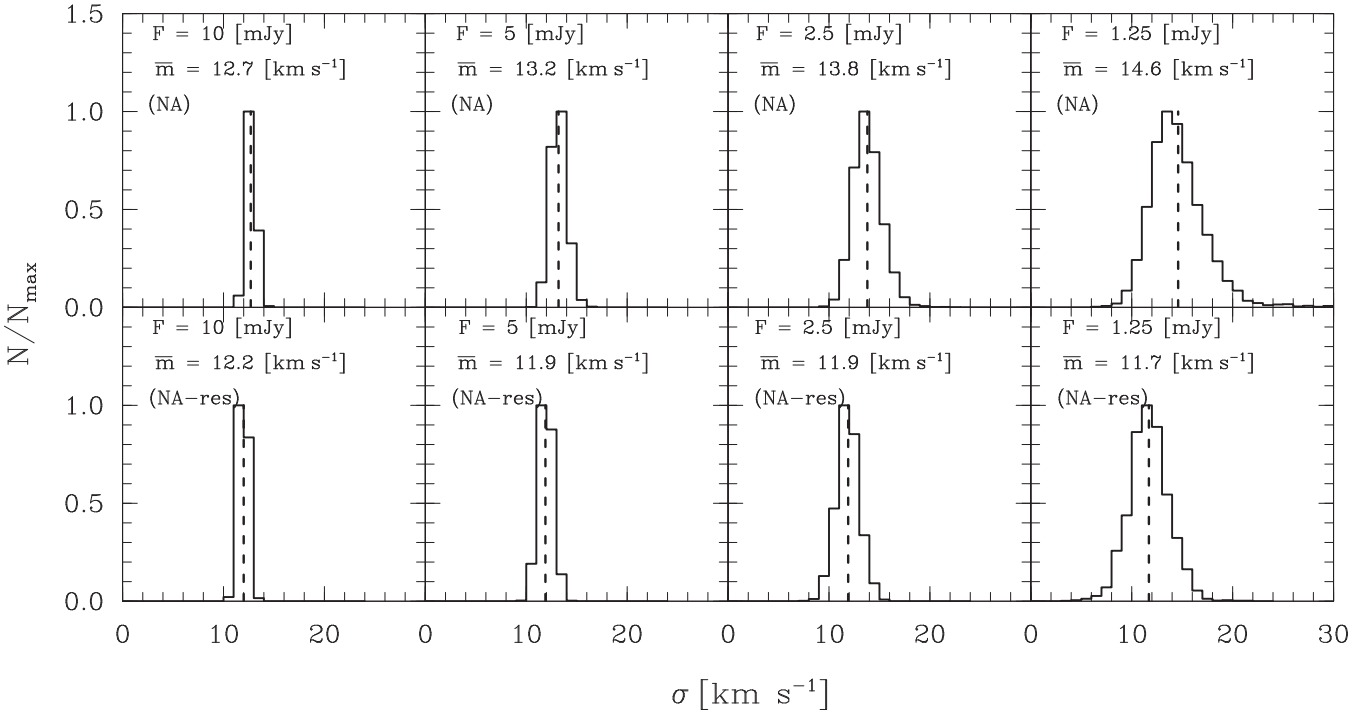

Figure 10. Histograms of single Gaussian velocity dispersions from natural non-residual (NA, first four panels) and natural residual-scaled (NA-res, last four panels) model data cubes. F: input peak flux; $\bar{m}$: output mean velocity dispersion; vertical dashed lines: input velocity dispersion (12 km s^{-1}) used to make the models.

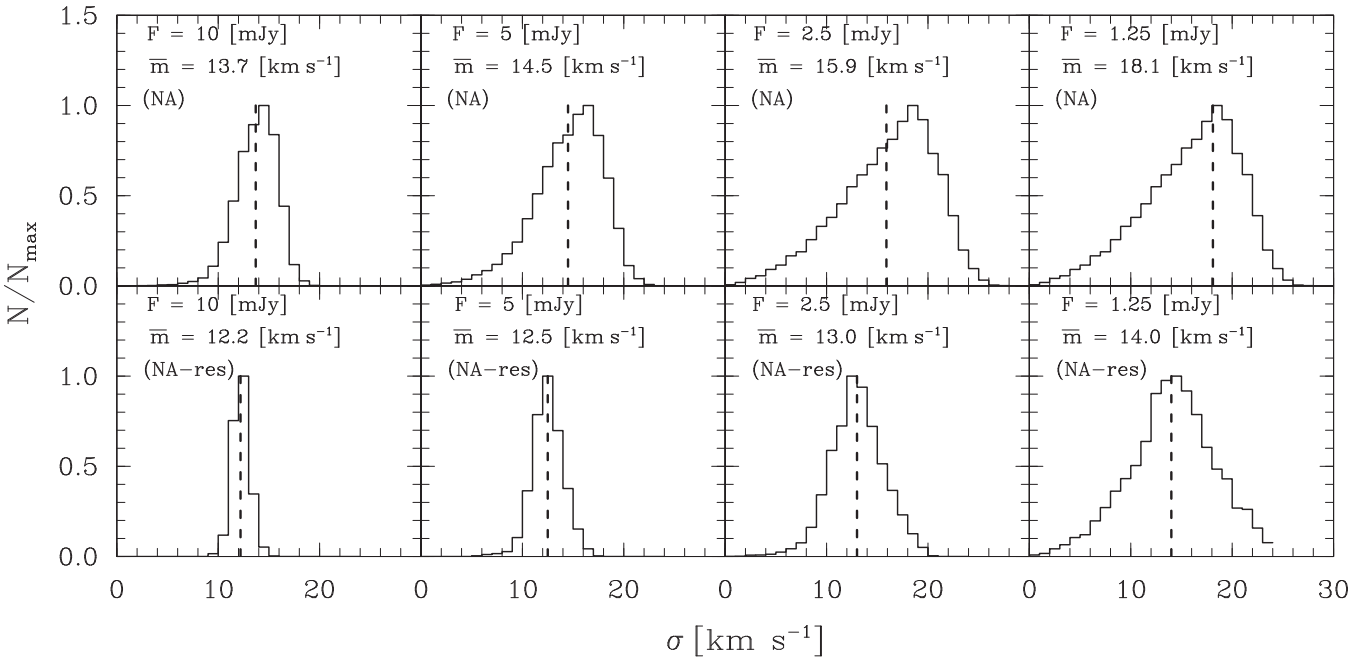

Figure 11. Histograms of second moment values from the natural non-residual-scaled (NA, first four panels) and natural residual-scaled (NA-res, last four panels) scaled model data cubes. F: input peak flux; $\bar{m}$: output mean velocity dispersion; vertical dashed lines: input velocity dispersion (12 km s^{-1}) used to make the models.

using second moment calculation and single Gaussian fits of H I spectra. Here, the model cubes created using the above procedure all have Gaussian input spectra with a velocity dispersion of 12 km s^{-1}, but different peak flux values.

Figures 10 and 11 show histograms of the single Gaussian dispersion and the mean second moment values derived from the model data cubes. We use the GIPSY task MOMENTS to calculate the second moment values. We do not apply any restrictions, such as clipping of spectral channels, to derive the second moment values. The model cubes do not contain any double profiles or large noise spikes, so the values shown in Figures 10 and 11 are not affected by this. For the non-residual-scaled cubes, the velocity dispersions from both the single Gaussian fits and the second moment maps depend on the input peak flux. The derived mean velocity dispersions tend to increase from higher to lower S/N. For the lowest input peak flux, the mean single Gaussian dispersion and second moment values differ from the input dispersion by ∼18% and ∼34%,

Table 2
Parameters from Different Set of Model Data Cubes I

Non-residual Scaled					Residual-scaled				
σ_n (km s^{-1})	σ_b (km s^{-1})	Peak Flux (mJy)	a_n/a_b	A_n/A_b	σ_n (km s^{-1})	σ_b (km s^{-1})	Peak Flux (mJy)	a_n/a_b	A_n/A_b
1	2	3	4	5	6	7	8	9	10
8.00	**20.00**	**10.00**	**1.50**	**0.60**	**8.00**	**20.00**	**10.00**	**1.50**	**0.60**
8.17 ± 0.06	22.19 ± 0.28	11.45	1.53 ± 0.03	0.56 ± 0.03	7.98 ± 0.04	19.63 ± 0.16	11.12	1.51 ± 0.02	0.61 ± 0.03
8.00	**20.00**	**5.00**	**1.50**	**0.60**	**8.00**	**20.00**	**5.00**	**1.50**	**0.60**
8.32 ± 0.12	23.35 ± 0.57	5.99	1.44 ± 0.04	0.51 ± 0.05	7.97 ± 0.09	19.33 ± 0.30	5.54	1.50 ± 0.05	0.62 ± 0.06
8.00	**20.00**	**2.50**	**1.50**	**0.60**	**8.00**	**20.00**	**2.50**	**1.50**	**0.60**
8.24 ± 0.25	23.48 ± 0.99	3.25	1.21 ± 0.07	0.42 ± 0.08	7.94 ± 0.18	18.92 ± 0.60	2.75	1.48 ± 0.10	0.62 ± 0.12
8.00	**20.00**	**10.00**	**2.33**	**0.93**	**8.00**	**20.00**	**10.00**	**2.33**	**0.93**
8.15 ± 0.05	22.65 ± 0.35	11.45	2.29 ± 0.04	0.82 ± 0.05	7.98 ± 0.04	19.50 ± 0.21	11.12	2.35 ± 0.04	0.96 ± 0.05
8.00	**20.00**	**5.00**	**2.33**	**0.93**	**8.00**	**20.00**	**5.00**	**2.33**	**0.93**
8.23 ± 0.10	23.77 ± 0.73	5.99	2.08 ± 0.06	0.72 ± 0.08	7.98 ± 0.08	19.20 ± 0.41	5.54	2.35 ± 0.09	0.98 ± 0.11
8.00	**20.00**	**2.50**	**2.33**	**0.93**	**8.00**	**20.00**	**2.50**	**2.33**	**0.93**
8.19 ± 0.19	23.39 ± 1.10	3.25	1.69 ± 0.09	0.59 ± 0.11	7.96 ± 0.15	18.80 ± 0.79	2.75	2.34 ± 0.18	0.99 ± 0.22
Parameters from Different Set of Model Data Cubes II									
6.00	**16.00**	**10.00**	**1.49**	**0.56**	**6.00**	**16.00**	**10.00**	**1.49**	**0.56**
6.16 ± 0.04	17.89 ± 0.14	11.45	1.56 ± 0.02	0.54 ± 0.02	6.00 ± 0.03	15.76 ± 0.10	11.06	1.56 ± 0.02	0.59 ± 0.02
6.00	**16.00**	**5.00**	**1.49**	**0.56**	**6.00**	**16.00**	**5.00**	**1.49**	**0.56**
6.20 ± 0.09	18.39 ± 0.33	5.99	1.42 ± 0.04	0.48 ± 0.04	6.01 ± 0.06	15.61 ± 0.20	5.51	1.56 ± 0.04	0.60 ± 0.05
6.00	**16.00**	**2.50**	**1.49**	**0.56**	**6.00**	**16.00**	**2.50**	**1.49**	**0.56**
6.15 ± 0.22	18.45 ± 0.64	3.25	1.19 ± 0.07	0.40 ± 0.08	6.04 ± 0.12	15.52 ± 0.38	2.73	1.60 ± 0.08	0.62 ± 0.09
6.00	**16.00**	**1.25**	**1.49**	**0.56**	**6.00**	**16.00**	**1.25**	**1.49**	**0.56**
5.97 ± 0.47	17.67 ± 1.01	1.84	0.92 ± 0.11	0.31 ± 0.12	6.13 ± 0.23	15.66 ± 0.77	1.34	1.71 ± 0.17	0.67 ± 0.20
6.00	**16.00**	**10.00**	**2.32**	**0.87**	**6.00**	**16.00**	**10.00**	**2.32**	**0.87**
6.12 ± 0.04	18.15 ± 0.21	11.45	2.33 ± 0.04	0.78 ± 0.04	6.00 ± 0.03	15.70 ± 0.13	11.06	2.43 ± 0.04	0.93 ± 0.04
6.00	**16.00**	**5.00**	**2.32**	**0.87**	**6.00**	**16.00**	**5.00**	**2.32**	**0.87**
6.16 ± 0.08	18.62 ± 0.42	5.99	2.06 ± 0.06	0.68 ± 0.07	6.02 ± 0.05	15.59 ± 0.26	5.51	2.47 ± 0.08	0.95 ± 0.09
6.00	**16.00**	**2.50**	**2.32**	**0.87**	**6.00**	**16.00**	**2.50**	**2.32**	**0.87**
6.13 ± 0.19	18.29 ± 0.79	3.25	1.68 ± 0.11	0.56 ± 0.12	6.06 ± 0.10	15.54 ± 0.50	2.73	2.56 ± 0.15	1.00 ± 0.17
6.00	**16.00**	**1.25**	**2.32**	**0.87**	**6.00**	**16.00**	**1.25**	**2.32**	**0.87**
6.01 ± 0.43	17.08 ± 1.23	1.84	1.28 ± 0.17	0.45 ± 0.19	6.10 ± 0.19	15.67 ± 1.00	1.34	2.73 ± 0.32	1.06 ± 0.36
6.00	**16.00**	**10.00**	**0.80**	**0.30**	**6.00**	**16.00**	**10.00**	**0.80**	**0.30**
6.25 ± 0.07	17.59 ± 0.13	11.45	0.88 ± 0.01	0.31 ± 0.02	5.99 ± 0.04	15.80 ± 0.08	11.06	0.82 ± 0.01	0.31 ± 0.01
6.00	**16.00**	**5.00**	**0.80**	**0.30**	**6.00**	**16.00**	**5.00**	**0.80**	**0.30**
6.33 ± 0.12	18.24 ± 0.24	5.99	0.83 ± 0.02	0.29 ± 0.03	5.99 ± 0.09	15.67 ± 0.14	5.51	0.82 ± 0.02	0.31 ± 0.02
6.00	**16.00**	**2.50**	**0.80**	**0.30**	**6.00**	**16.00**	**2.50**	**0.80**	**0.30**
6.21 ± 0.26	18.55 ± 0.46	3.25	0.72 ± 0.04	0.24 ± 0.05	6.02 ± 0.17	15.52 ± 0.27	2.73	0.82 ± 0.04	0.32 ± 0.05
6.00	**16.00**	**1.25**	**0.80**	**0.30**	**6.00**	**16.00**	**1.25**	**0.80**	**0.30**
5.91 ± 0.57	18.14 ± 0.76	1.84	0.55 ± 0.06	0.18 ± 0.07	6.13 ± 0.32	15.52 ± 0.54	1.34	0.86 ± 0.08	0.34 ± 0.10

Note. The input parameters for each model are represented in bold, whereas the derived parameters from the resulting cubes are shown in regular font. Columns 1 and 6: velocity dispersion of the narrow component; Columns 2 and 7: velocity dispersion of the broad component; Columns 3 and 8: input peak flux values; Columns 4 and 9: ratio between the input amplitude of the narrow and the broad components. Columns 5 and 10: flux ratio of the narrow component and the broad component.

respectively. For the residual-scaled model data cubes, the mean single Gaussian velocity dispersions are very similar to the input dispersion. We do, however, observe a steady increase in the mean second moment values as we decrease the input peak flux values. The derived value differs from the input dispersion by ∼14% at the lowest input peak flux. The histograms of the second moment values have a broader distribution compared to those of the single Gaussian dispersions, especially for the non-residual-scaled cubes at low S/N. Thus, second moment values are more sensitive to S/N than single Gaussian dispersions. The effects of S/N are more pronounced for the non-residual-scaled than for the residual-scaled cubes. The results from the models show that for the standard THINGS cubes (i.e., cleaned to 2.5 time the rms noise), residual-scaled cubes give more accurate velocity dispersion as opposed to non-residual-scaled cubes. The latter tend to overestimate the velocity dispersions, especially in the low S/N regime.

5.2. Effects of Residual Scaling on Velocity Dispersions Derived from a Fitted Two-Gaussian Model

Here, the model data cubes are constructed using narrow and broad Gaussian input spectra, each with different input profile parameter values (σ_n, σ_b, A_n/A_b, and the ratio of the narrow and broad component amplitudes, a_n/a_b). Table 2 illustrates the results from the various models, where the input parameters are shown in bold. The conclusions can be summarized as follows. The residual and non-residual-scaled model data cubes give similar σ_n values, approaching the input values for a range of S/N. However, the non-residual-scaled cubes give σ_b values that are overestimated by up to ∼16%, whereas the residual-scaled ones result in σ_b values similar to the input values. In

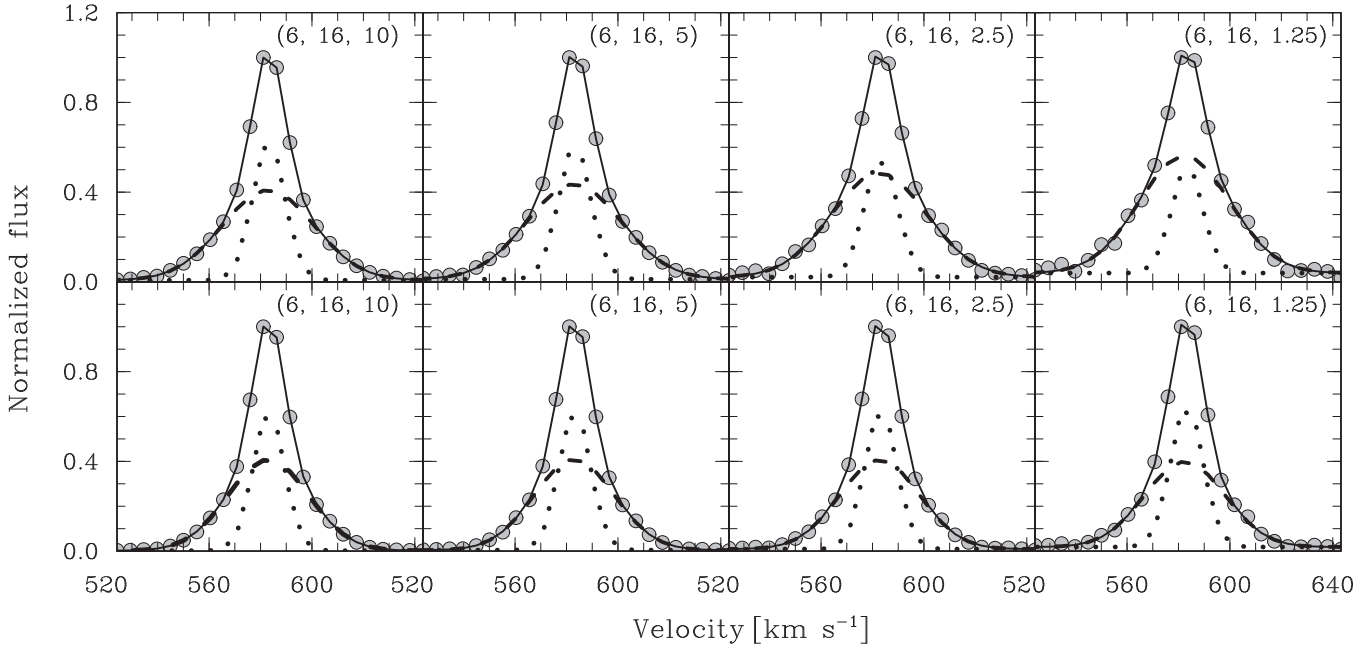

Figure 12. Synthetic super profiles from non-residual-scaled cubes (top panels) and residual-scaled cubes (bottom panels). The numbers in each plots are the input σ_n (km s^{-1}), σ_b (km s^{-1}), and peak flux (i.e., $a_n + a_b$ in mJy) values.

addition, the non-residual-scaled cubes tend to underestimate the A_n/A_b ratios, especially for lower input peak flux values (i.e., lower S/N). The derived A_n/A_b values from the residual-scaled cubes, however, are similar to the input values and do not depend on the input peak flux. For the non-residual scaled cubes, when we go from higher to lower input peak flux, the σ_n and σ_b values stay basically the same, whereas the broad component amplitude becomes higher and therefore its area also gets larger. This results in a decrease in the a_n/a_b and A_n/A_b ratios. Thus in the low S/N regime, the A_n/A_b ratio from non-residual-scaled cubes can be underestimated. For example, in our model, where the S/N is ∼3.6, A_n/A_b is underestimated by up to ∼48%. For the residual-scaled cubes, the derived A_n/A_b ratios and the input values agree within ∼18% for the same S/N. To illustrate these, we show the shapes of the (overall) super profiles, the individual narrow and broad components in Figure 12 for a range of S/N for both the residual and the non-residual-scaled cubes. Figure 12 clearly shows that the amplitudes of the fitted narrow and broad components from the non-residual-scaled cubes are sensitive to the input S/N. However, the shapes of the fitted narrow/broad components from the residual-scaled cubes are not dependent on the input S/N.

6. Discussion and Conclusion

We have shown that, for observations where the shape of the dirty beam deviates significantly from that of a Gaussian, H I velocity dispersion is sensitive to cleaning depth. If the dirty beam has prominent wings and if not very deeply cleaned, the cleaned map will consist of cleaned emission with a Gaussian beam sitting on a broad pedestal residual emission. Second moment values and broad component dispersions derived from such cubes will be overestimated as they are sensitive to profile wings. Blanking also affects the broad profile wings. The narrow component flux and dispersion are, however, not affected by the dirty beam effects as they represent the core of the profile which is mostly composed of bright emission that is properly cleaned. The mismatch between the dirty beam and the fitted clean beam also leads to smaller σ_n/σ_b and A_n/A_b values. Analogous to the narrow component, the single Gaussian dispersions are less overestimated as the fitting routine tends to fit the core of the profiles.

Robust weighting is less dependent on cleaning depth because the resulting dirty beam has less prominent wings. However, as seen in Section 3, the natural dirty beam can be substantially different from the fitted restoring beam. The effects of this mismatch on the estimate of H I flux and velocity dispersion can be lowered by scaling the residuals by the ratio between the clean beam area and the dirty beam area (see also Stilp et al. 2013). This is why the super profiles from residual-scaled cubes tend to have smaller wings than those from non-residual-scaled cubes as seen in Figure 9. This implies that for arrays where the dirty beam is more Gaussian (e.g., the WSRT telescope) these effects are less prominent to absent. In conclusion, when dealing with observations where the dirty beam is significantly non-Gaussian (e.g., of multi-configuration VLA observations), we recommend the use of residual-scaled cubes or cubes that are cleaned close to the noise level (1.5 times the rms noise or deeper) for H I velocity dispersion analysis. Cleaning to insufficient depth can lead to a significant misestimate of the velocity dispersion. While cleaning this deep is not always trivial for the classical CLEAN, it has been shown that the MSCLEAN algorithm does well in cleaning close to the noise level (Rich et al. 2008), without suffering from divergence.

We thank the anonymous referee for useful and constructive comments. We are also grateful to Dr. Fabian Walter for useful discussions during the preparation of this manuscript.

R.I. acknowledges funding from the Alexander von Humboldt foundation through the Georg Forster Research Fellowship program.

R.I.'s working visit to the Netherlands was supported by the South African National Research Foundation-Netherlands Organisation for Scientific Research (NRF-NWO) exchange

programme in "Astronomy, and Enabling Technologies for Astronomy."

The work of W.J.G.dB. was supported by the European Commission (grant FP7-PEOPLE-2012-CIG #333939).

References

Braun, R. 1997, ApJ, 484, 637
Briggs, D. S. 1995, AAS Meeting 187 Abstracts, #112.02
Cannon, J. M., Giovanelli, R., Haynes, M. P., et al. 2011, ApJL, 739, L22
Cornwell, T. J. 2008, ISTSP, 2, 793
Högbom, J. A. 1974, A&AS, 15, 417
Hunter, D. A., Ficut-Vicas, D., Ashley, T., et al. 2012, AJ, 144, 134
Ianjamasimanana, R., de Blok, W. J. G., Walter, F., et al. 2012, AJ, 144, 96
Jorsater, S., & van Moorsel, G. A. 1995, AJ, 110, 2037
O'Brien, J. C., Freeman, K. C., & van der Kruit, P. C. 2010, A&A, 515, 62
Ott, J., Stilp, A. M., Warren, S. R., et al. 2012, AJ, 144, 123
Petric, A. O., & Rupen, M. P. 2007, AJ, 134, 1952
Rich, J. W., de Blok, W. J. G., Cornwell, T. J., et al. 2008, AJ, 136, 2897
Schaye, J. 2004, ApJ, 609, 667
Stilp, A. M., Dalcanton, J. J., Warren, S. R., et al. 2013, ApJ, 765, 136
Tamburro, D., Rix, H.-W., Leroy, A. K., et al. 2009, AJ, 137, 4424
Walter, F., Brinks, E., de Blok, W. J. G., et al. 2008, AJ, 136, 2563
Yatawatta, S. 2014, MNRAS, 444, 790
Young, L. M., van Zee, L., Lo, K. Y., et al. 2003, ApJ, 592, 111